2020 5th International Conference on Advanced
Robotics and Mechatronics (ICARM)

Design and Control of an Index Finger Exoskeleton with Cable-Driven Translational Joints

Houcheng Li, Long Cheng and Zhengwei Li

***Abstract*— This paper proposes a new cable-driven wearable index finger exoskeleton to exercise flexion and extension of the index finger. This exoskeleton adopts an opportune constraint planar four-bar mechanism with an actively driving translational joint to reduce vertical space occupation and to achieve joint axis alignment for human-robot kinematic compatibility. The mechanical structure of the proposed exoskeleton is further optimized to minimize the exoskeleton's volume. The proposed exoskeleton is fabricated by 3D printing, has two active degrees of freedom (DoFs) configured in the metacarpophalangeal (MCP) and proximal interphalangeal (PIP) joints individually, and can be easily worn by buckling the Velcro straps. Moreover, to ensure patients move their fingers freely after powering down, a decoupling mechanism is designed to remove the coupling between the motor and the exoskeleton. Due to the fact that the human's hand main tremble unconsciously or pick up a load suddenly, such unexpected disturbances may influence the control performance of the proposed exoskeleton. To this end, the active disturbance rejection control (ADRC) algorithm is adopted to reduce the influence of external disturbances. Finally, the functionality of the proposed exoskeleton is verified by experiments, and the experiments also validate the performance of the ADRC algorithm by comparing to the traditional proportional control.**

I. Introduction

Stroke is the second most common cause of death and the major cause of disability worldwide [1]. Most of the post-stroke patients usually lose total or partial hand movement ability [2], whose activities of daily living (ADL) are significantly affected. Therefore, regaining hand function by rehabilitation practice is considered one most critical needs. However, the number of rehabilitation therapists is too insufficient to meet the large requirement in the market.

Fortunately, many hand exoskeletons have been developed to help therapists do rehabilitation and assist the patient's ADL [3]–[5]. In the literature, the hand exoskeleton can be categorized into four types according to the driven manner: the linkage-driven exoskeleton, the pneumatic-driven exoskeleton, the tendon-driven exoskeleton, and the cable-driven exoskeleton. The linkage-driven hand exoskeleton has some advantages such as higher force transmission efficiency, greater force, and easier to control, however, this exoskeleton is normally too bulky and heavy to be conveniently used because the wearable parts and motors are coupled together [6]–[8]. To improve the compactness and reduce the weight of the exoskeleton, the pneumatic-driven exoskeleton is designed, which is usually fabricated by elastomeric materials and pneumatically actuated [9]–[11]. Due to the low elastic modulus, this exoskeleton tends to be more comfortable, and easier to achieve the alignment of the finger joint axis. However, there is no free lunch, providing great force and being controlled precisely are difficult for the pneumatic-driven exoskeleton. Moreover, the pneumatic-driven exoskeleton requires an air pump or compressor, which would make some noises and limit the portability of the whole system. To contract the above problems and reserve the soft characteristic simultaneously, the tendon-driven exoskeleton has been proposed [12]–[15]. This exoskeleton is more compact and portable. Nevertheless, to achieve hand flexion movement, this exoskeleton needs a tendon placed in the palm to pull impairment finger, which affects the user's object grasping and manipulation in ADL. Besides, these tendons are usually fixed in a glove, which brings inconvenience when wearing the exoskeleton by post-stroke patients with spasticity. For the sake of balancing the advantages and disadvantages of the above exoskeletons, the cable-driven exoskeleton has been developed [16]–[21]. This exoskeleton could provide enough force for hand rehabilitation and operation, and the wearable parts have low weight because the driven parts are placed away from the hand. Moreover, to increase the compliance, the serial elastic actuation has been used to bring passive compliance except for the active compliance control [22]. However, there are two points possibly overlooked in the design of the cable-driven exoskeletons. One point is the wearable parts of the

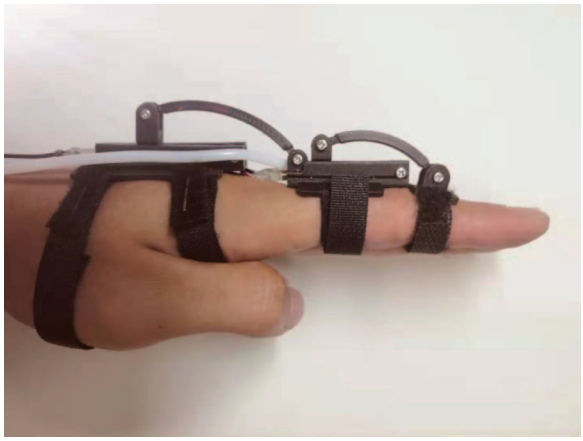

Fig. 1. The overall appearance of the proposed index finger exoskeleton.

This work was supported in part by the National Natural Science Foundation of China (Grants 61873268 and 61633016) and Beijing Natural Science Foundation (Grant L182060).

H. Li, L. Cheng and Z. Li are all with the State Key laboratory of Management and Control for Complex Systems, Institute of Automation, Chinese Academy of Sciences, Beijing 100190, China. The authors are also with the School of Artificial Intelligence, University of Chinese Academy of Sciences, Beijing 100049, China. Email: long.cheng@ia.ac.cn.

cable-driven exoskeletons normally occupy too much vertical space above the hand. Therefore, these exoskeletons look lager, which would bring inconvenience to patients when using it. Another point is the patient cannot move his/her finger freely while wearing the exoskeletons after powering down, however, moving fingers freely is beneficial for the active rehabilitation training and could protect the patients from the secondary injury when an emergency power failure occurs.

By the above observations, one purpose of this study is to design a low vertical space occupation and light-weight index finger exoskeleton to help post-stroke patients do hand rehabilitation training or assist the patients' ADL. To this purpose, an opportune constraint planar four-bar mechanism with an actively driving translational join is designed, and the mechanical structure is also optimized to minimize the exoskeleton size. The proposed exoskeleton is driven by cables and fabricated by the 3D printing technology. This exoskeleton can provide two active degrees of freedom (DoF) configuring in metacarpophalangeal (MCP) and proximal interphalangeal (PIP) of the index finger, which can be worn by buckling the Velcro strap. Another purpose of this study is to design a decoupling mechanism to decouple the motor and the exoskeleton, which could ensure the proposed exoskeleton could move freely after powering down. The last purpose of this study is to achieve precise control under external disturbances, which can be fulfilled by employing the active disturbance rejection control (ADRC) proposed in [23], [24].

To summarize, the main contributions of this paper can be stated as follows

1) From the mechanical design point of view, compared to other cable-driven exoskeletons [19]–[21], the mechanical design of the proposed exoskeleton adopts an opportune constraint planar four-bar mechanism with an actively driving translational joint instead of actively driving the rotational joint. This design makes full use of the horizontal space of the finger and reduces the use of vertical space above the finger, which makes the exoskeleton smaller in size. Meanwhile, this mechanical design of actively driving the translational joint also brings benefits to control.
2) From the safety point of view, this paper proposes a decoupling mechanism to realize the patients' finger free movement when wearing the exoskeleton after powering off, which can not only guarantee the active movement of the finger but also increases the security of the exoskeleton.
3) From the control algorithm point of view, this paper adopts the ADRC control algorithm to obtain a better control performance when facing different disturbances in the system. Comparing to the traditional proportional control algorithm, the ADRC algorithm is more preferable to the proposed exoskeleton.

The rest of this paper is organized as follows. Section II introduces the design of the proposed index finger exoskeleton and the decoupling mechanism as well as the calibration of sensors. In Section III, the ADRC control algorithm is presented. Section IV describes experiments for validating the mechanical design and control algorithm. Finally, Section V concludes this study and presents the future work plan.

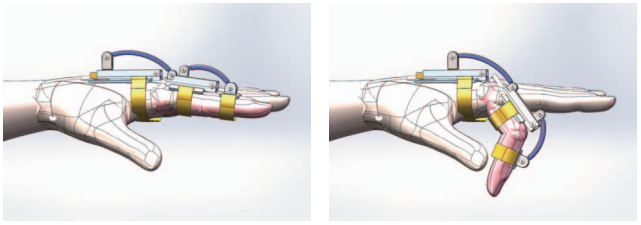

(a) Index finger extension. (b) Index finger flexion.

Fig. 2. An animated demonstration of how the proposed index finger exoskeleton works.

II. Mechanical Design

A. Design of Hand Exoskeleton

The overall appearance of the proposed index exoskeleton is illustrated in Fig. 1. In terms of the finger movement, breaking the simultaneous movement of the MCP and PIP joints is beneficial to motor learning [22]. Moreover, the exoskeleton with independent movement at MCP and PIP joints would be more versatile, which would help patients complete multiple hand rehabilitation training or enhance operational capabilities effectively. Therefore, the proposed index finger exoskeleton has independent DoFs at the MCP and PIP joints. Meanwhile, because there exists the anatomical coupling between the PIP joint and the distal interphalangeal (DIP) joint, the exoskeleton has no DoF at the DIP joint. Through these DoFs' configuration, the flexion and extension movements are implemented in this paper. To achieve the joint axis alignment, the mechanical structures of both MCP and PIP joints include the opportune constraint planar four-bar mechanisms that are composed of three rotational joints and one translational joint. In order to make full use of the horizontal space of the finger and to reduce the use of the vertical space above the finger, the translational joint is driven actively to achieve the flexion and extension movements of the MCP and PIP joints. Figure 2 presents an animated demonstration revealing the extension and flexion movements of the index finger while wearing the proposed exoskeleton.

The design details of the proposed exoskeleton are shown in Fig. 3 by an exploded view of the Solidworks model. Three details need to be highlighted in the design. First, the proposed exoskeleton employs the cable-driven manner to drive the translational joint (slider) bidirectionally. Second, to further reduce the space occupation, the proposed exoskeleton only uses one cable sheath placed on the back end of the translational joint. The fixed pulley placed on the front end of the translational joint is used to change the forward direction to the backward direction. Third, the displacement sensor fixed on the side of the slider is designed to detect the slider's position. This sensor is based on the resistance

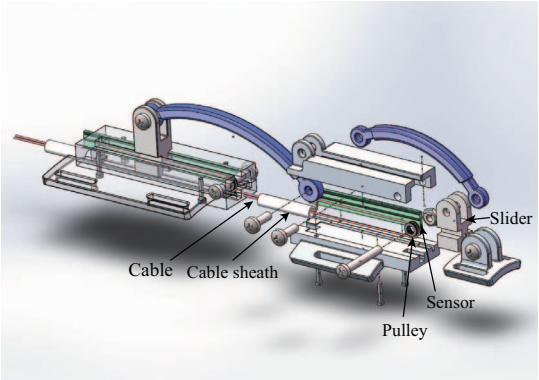

Fig. 3. Exploded view of the proposed index finger exoskeleton's Solidworks model

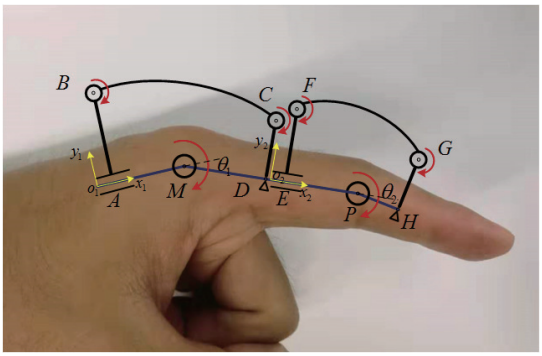

Fig. 4. The kinematic model's parameters of the proposed index finger exoskeleton. The arrows in yellow represent the coordinate frames for the MCP and PIP joints. The circles in red depict the revolute joints.

principle. The slider and the sensor are connected by a metal sheet. When the slider moves in the chute, the resistance of the displacement sensor changes such that the slider position could be detected by reading the resistance value. Therefore, the finger's joint angle could be calculated by the kinematics of the proposed exoskeleton.

To make the proposed exoskeleton as small and light as possible while still satisfying the maximum angle of the finger movement, optimizing the proposed exoskeleton structure is necessary. The kinematic parameters of the proposed index finger exoskeleton are shown in Fig. 4. Taking the PIP joint exoskeleton as an example, the coordinate frame is located at the point o_2 which is related to the wear position, and the kinematic model for the closed-loop PIP chain is written with the exponential expression as follows

$$l_{EF}e^{i90^\circ} + l_{FG}e^{i\theta_F} + l_{GH}e^{i\theta_G} = X_{EP}e^{i0^\circ} + l_{PH}e^{i\theta_2}, \quad (1)$$

where l_{EF}, l_{FG}, l_{GH}, and l_{PH} are the lengths of the links EF, FG, GH, and PH, respectively. X_{EP} presents the length between the translational joint (slider) and the PIP joint. θ_F and θ_G are the angles between FG, GH and the x_2-axis, respectively. θ_2 presents the angle of the PIP joint. Through solving the above kinematic equation in MATLAB, the solution can be expressed as $\theta_2 = f(X_{EP})$. The singularity occurs when there is no solution to the above equation, and the singularity takes the form of F, G, and P being collinear.

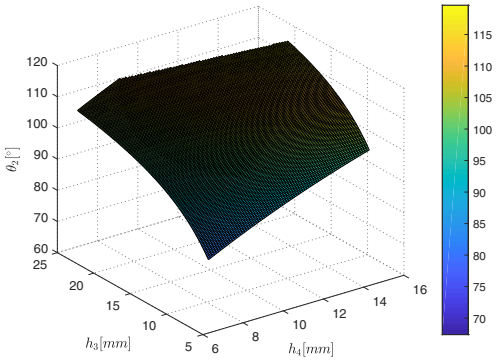

Fig. 5. Optimization result of the proposed exoskeleton mechanical structure

In the optimization, the length of the proximal phalanx and the length of the middle phalanx are measured to be 50mm and 28mm, respectively. The optimization of the linkage length could be expressed as follows

$$\begin{aligned} \min \quad & f = l_{EF} + l_{GH} \\ s.t. \quad & 0 \le l_{EF} \le 50, \\ & 0 \le l_{GH} \le 50, \\ & 0 \le X_{EP} \le 50, \\ & 0 \le l_{PH} \le 28, \\ & \theta_2 = 90^\circ. \end{aligned} \quad (2)$$

Figure 5 presents the relationship between h_3, h_4 with θ_2, h_3 and h_4 are finally optimized to be 15mm and 10mm, respectively. Comparing to [21], [22], the proposed design reduces the vertical space occupation and makes full use of the horizontal space of the finger.

B. Design of Decoupling Mechanism

Inspired by the working principle of the car clutch, the decoupling mechanism is designed to disconnect the proposed exoskeleton from the motor. Its main components are marked in Fig. 6. The input axle of the decoupling mechanism is connected with the motor axle, and these two axles are coaxial and locked. When the power of the exoskeleton system is off, the spring force pushes the winding pulley from the input axle. At this time, the winding pulley can follow the free movement of the proposed exoskeleton. While the exoskeleton system is powered on, the suction-cup electromagnets attract iron sheets under the action of the magnetic field. The iron sheets move towards the direction of the pulley, which generates the propulsive force on the pulley by the bearing transmission. Meanwhile, the pulley compresses the spring under the propulsive force until it connects the input axle, and the spring is compressed in the cavity of the pulley and the input axle. When designing the winding pulley and the input axle, there are corresponding coupling teeth on their contact surfaces. At this time, the corresponding coupling teeth on their contact surfaces are coupled together. Under the frictional force, the winding

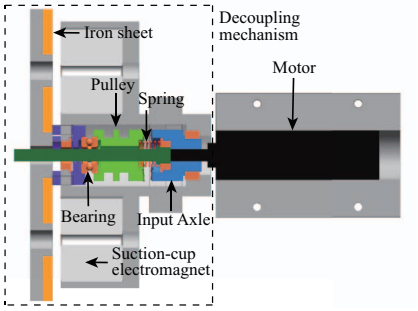

(a) Decoupling the proposed exoskeleton with the motor after powering down.

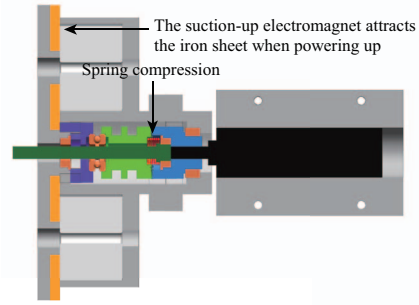

(b) Coupling the proposed exoskeleton with the motor after powering up.

Fig. 6. The Solidworks model of the proposed decoupling mechanism and its working principle.

pulley rotates with the input axle. The exoskeleton and the motor are coupled together, and the patient's finger can move along with the exoskeleton driven by the motors. Therefore, this decoupling mechanism could realize the free movement of the exoskeleton when powering down, and achieve the finger's passive movement when powering on. On the contrary, if the cable-driven exoskeleton does not have the decoupling mechanism, the exoskeleton could not move freely when powering down due to the high reduction ratio of the motor gearbox. This is not beneficial to the patient's active finger training and may cause secondary injury when an emergency power failure occurs.

C. Calibration of Sensors

To calculate the finger joint's angle accurately, the proposed displacement sensor is calibrated by a commercial data glove (WISEGOLVE15, a product of WONSTAR company). In the calibration experiment, the commercial data glove is worn on the volunteer's hand first, and then the proposed index finger exoskeleton is worn outside of the glove. Through the serial port which collects both the data of the exoskeleton and the glove simultaneously, the 4-order polynomial curve fitting of the displacement sensor is implemented for the calibration. Taking the DIP joint as an example, the curve fitting result is shown in Fig. 7. The equation of the polynomial curve fitting is described as follows

$$y = 356.8x^4 - 2734x^3 + 7733x^2 - 9487x + 4257, \quad (3)$$

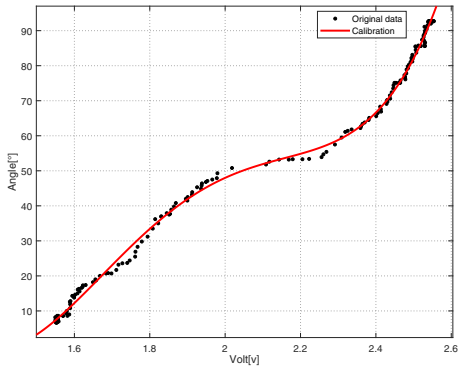

Fig. 7. The 4-order polynomial curve fitting for the proposed displacement sensor data by a commercial data glove.

where x represents the slider position measured by the proposed sensor and y is the DIP joint's angle.

III. Control Algorithm

The control objective is to reduce the position error between the predesigned finger joint angle and the actual finger joint angle. First, the PID control is employed for controlling the index finger joint angle. It has been experimentally verified that using the proportional control can control the exoskeleton well. This proportional controller is expressed as follows

$$u(t) = k_p(r - y(t)), \quad (4)$$

where $u(t)$ represents the proportional controller output, r is the reference representing the predesigned finger angle, $y(t)$ is the actual finger angle calculated by (3), k_p is the proportional coefficient selected by the trial-and-error approach. However, it should be noted that the human hand may tremble unconsciously or the human hand needs to pick up a load suddenly during the hand motion. The unexpected disturbances must be considered in the controller design. It is well known that the PID control has a very limited disturbance rejection ability.

Fortunately, the ADRC algorithm is proposed to reject disturbances (both internal and external disturbances), which does not require an exact system model. Instead, rough system identification is sufficient. The step-response experiment has been conducted to obtain a rough model of the exoskeleton which is described by the following first-order differential equation

$$\dot{y}(t) + ay(t) = bu(t), \qquad a, b > 0, \quad (5)$$

where $y(t)$ is the finger joint angle, $u(t)$ is the controller output. The a and b are identified as 0.554 and 0.472, respectively.

Let the external disturbance be denoted by ϵ. Then (5) can be rewritten by the following equation

$$\dot{y}(t) = -ay(t) + \epsilon + bu(t) = \delta(t) + bu(t), \quad (6)$$

where $\delta(t) = -ay(t) + \epsilon$ refers to the generalized distur-

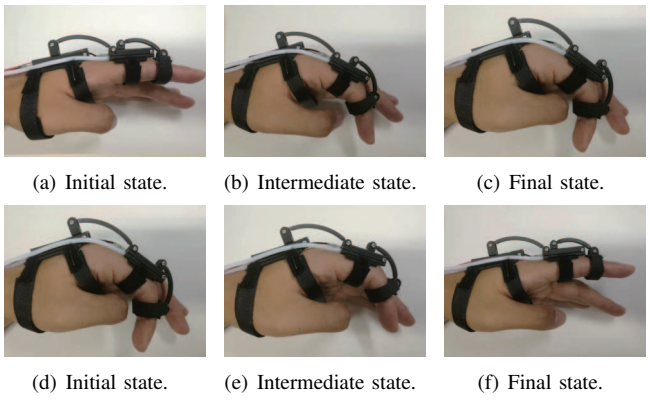

(a) Initial state. (b) Intermediate state. (c) Final state.

(d) Initial state. (e) Intermediate state. (f) Final state.

Fig. 8. Snapshots of the index finger's movement: from the extension status to the flexion status, and from the flexion status to the extension status.

bance. The essence of the ADRC algorithm is to obtain the estimation of $\delta(t)$, $\hat{\delta}(t)$, and employ its estimation $\hat{\delta}(t)$ in the control law, i.e., $u(t) = (-\hat{\delta}(t) + u_0(t))/b$.

Equation (6) is further rewritten in the state-space form as follows

$$\begin{cases} \dot{x}_1(t) = \delta(t) + bu(t), \\ y(t) = x_1(t), \end{cases} \tag{7}$$

where $x_1(t)$ is the finger joint angle.

Based on (7), an extend state observer (ESO) is designed to estimate the $\delta(t)$ as follows

$$\begin{cases} \dot{z}_1(t) = z_2(t) + bu(t) + \beta_1(y(t) - z_1(t)), \\ \dot{z}_2(t) = \beta_2(y(t) - z_1(t)), \\ z_2(t) = \hat{\delta}(t), \\ u(t) = \dfrac{-z_2(t) - k_p(z_1(t) - r)}{b}, \end{cases} \tag{8}$$

where β_1, β_2 represent the parameters of the ESO, $\hat{\delta}(t)$ is the estimation of $\delta(t)$, and $u(t)$ is the ADRC control law.

The selection of β_1 and β_2 is suggested in [25], where the (β_1, β_2) are obtained from the system characteristic equation as follows

$$\lambda(s) = s^2 + \beta_1 s + \beta_2 = (s + \omega_0)^2, \quad \omega_0 > 0. \tag{9}$$

The control performance of the ADRC controller is to be presented in Section IV.

IV. Experimental Results and Discussions

In the experiment, the functionality of the proposed exoskeleton is tested first, which is shown in Fig. 8. From the experimental results, it can be seen that both the finger's extension movement and the flexion movement can be achieved. Figure 9 presents the mechanical optimization result. Through the optimization, the height of the exoskeleton is reduced by 37% comparing to no optimization. In the experiment, the proposed decoupling mechanism could realize the disconnection between the exoskeleton and the motor, whose overall appearance is illustrated in Fig 10.

The ADRC algorithm and the proportional control algorithm are programmed into a microcontroller (STM32F407)

Fig. 9. The mechanical structure optimization: the top one is the mechanical structure before optimization and the bottom one is the mechanical structure after optimization.

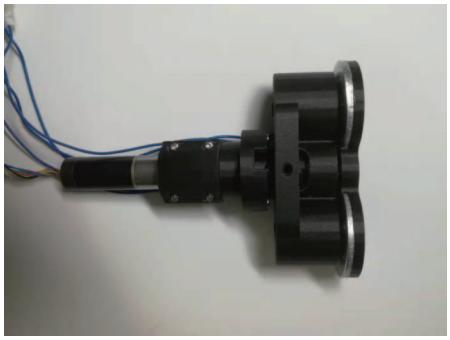

Fig. 10. The overall appearance of the proposed decoupling mechanism.

which sends commands to the brushless DC servo motors (1226A012B K1855, Faulhaber, Germany). In the experiment, the external disturbance is artificially added into the control input. This disturbance is applied at $t = 15$s . The control performance of the proposed ADRC controller is compared to the proportional controller, which is shown in Fig. 11. First, from the viewpoint of the steady-state performance, both controllers have a very small steady-state error. Second, from the perspective of the transient performance, the transient response time of the ADRC controller is 2.15s, and the transient response time of the proportional controller is 3.36s. The proposed ADRC controller is faster than the proportional controller. Third, from the standpoint of rejecting disturbances, when facing disturbance, the adjustment time of the proportional controller is 15.75s, and the proposed ADRC controller only requires 1.89s which proves its stronger ability in anti-disturbance. Therefore, the ADRC controller is a better solution for the proposed index finger exoskeleton with respect to the control performance.

V. Conclusion and Future Work

In this paper, a cable-driven index finger exoskeleton is designed based on an actively driven translational join. This design reduces the vertical space occupation and makes full use of the horizontal space. Meanwhile, this mechanical design is also optimized to reduce the exoskeleton's volume. A decoupling mechanism is designed to allow free motion of the finger when the exoskeleton has no power supply.

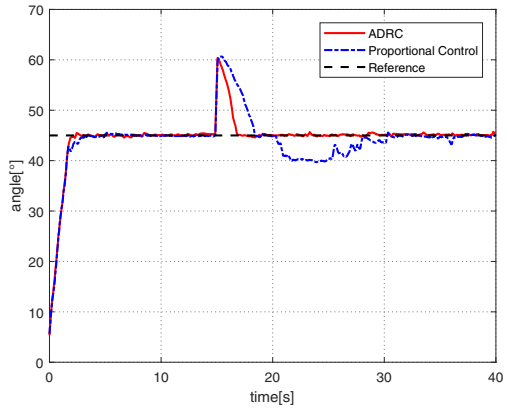

Fig. 11. Experimental result of the ADRC algorithm compared to the proportional control.

Moreover, the ADRC algorithm is employed to realize the control of the finger joint angle. Comparing to the proportional control, the proposed ADRC algorithm performs much better, which has been verified by the experiments.

The current work is mainly focused on the mechanical design and the position control. There are still many works needed to be accomplished in the future. First, the design of the entire hand exoskeleton (especially the thumb exoskeleton design) is required, and the other property (force or torque) of the proposed exoskeleton need to be considered in the optimization. Second, by following the similar idea presented in [26], the reduced ESO can be used to estimate the generalized disturbance instead of the standard ESO for simplifying the controller's complexity. Furthermore, the compliant force control needs to be realized in the proposed exoskeleton. Third, the clinical test should be conducted to verify the effectiveness of the proposed exoskeleton.

REFERENCES

[1] G.A. Donnan, M. Fisher, M. Macleod, and S.M. Davis, "Stroke," *The Lancet*, vol. 371, no. 9624, pp. 1612–1632, 2008.

[2] K.O. Thielbar, K.M. Triandafilou, H.C. Fischer, J.M. O'Toole, M.L. Corrigan, J.M. Ochoa, M.E. Stoykov, and D.G. Kamper, "Benefits of using a voice and EMG-driven actuated glove to support occupational therapy for stroke survivors," *IEEE Transactions Neural System Rehabilitation Engineering*, vol. 25, no. 3, pp. 297–305, 2017.

[3] D.T. Bundy, L. Souders, K. Baranyai, L. Leonard, G. Schalk, R. Coker, D.W. Moran, T. Huskey, and E.C. Leuthardt, "Contralesional brain-computer interface control of a powered exoskeleton for motor recovery in chronic stroke survivors," *Stroke*, vol. 48, no. 7, pp. 1908–1915, 2017.

[4] S.R. Soekadar, M. Witkowski, C. Gmez, E. Opisso, J. Medina, M. Cortese, M. Cempini, M.C. Carrozza, L.G. Cohen, N. Birbaumer, and N. Vitiello, "Hybrid EEG/EOG-based brain/neural hand exoskeleton restores fully independent daily living activities after quadriplegia," *Science Robotics*, vol. 1, no. 1, p. eaag3296, 2016.

[5] M. Mekki, A.D. Delgado, A. Fry, D. Putrino, and V. Huang, "Robotic rehabilitation and spinal cord injury: a narrative review," *Neurotherapeutics*, vol. 15, no. 3, pp. 604–617, 2018.

[6] M. Gabardi, M. Solazzi, D. Leonardis, and A. Frisoli, "Design and evaluation of a novle 5 DoF underactuated thumb-exoskeleton," *IEEE Robotics and Automation Letters*, vol. 3, no. 3, pp. 2322–2329, 2018.

[7] I. Jo and J. Bae, "Design and control of a wearable hand exoskeleton with force-controllable and compact actuator modules," in *Proceedings of 2015 IEEE International Conference on Robotics and Automation*, Seattle, USA, May 2015, pp. 5596-5601.

[8] Z. Lu, R.K. Tong, X. Zhang, S. Li, and P. Zhou, "Myoelectric pattern recognition for controlling a robotic hand: A feasibility study in stroke," *IEEE Transactions on Biomedical Engineering*, vol. 66, no. 2, pp. 365–372, 2019.

[9] H. Zhao, J. Jalving, R. Huang, R. Knepper, A. Ruina, and R. Shepherd, "A helping hand: soft orthosis with integrated optical strain sensors and EMG control," *IEEE Robotics and Automation Magazine*, vol. 23, no. 3, pp. 56–64, 2016.

[10] J. Wang, Y. Fei, and W. Pang, "Design, modeling, and testing of a soft pneumatic glove with segmented PneuNets bending actuators," *IEEE/ASME Transactions on Mechatronics*, vol. 24, no. 3, pp. 990–1001, 2019.

[11] H. Zhang, A.S. Kumar, F. Chen, J.Y.H. Fuh, and M.Y. Wang, "Topology optimized multimaterial soft fingers for applications on grippers, rehabilitation, and artificial hands," *IEEE/ASME Transactions on Mechatronics*, vol. 24, no. 1, pp. 120–131, Feb. 2019.

[12] S.W. Lee, K.A. Landers, and H.S. Park, "Development of a biomimetic hand exotendon device (BiomHED) for restoration of functional hand movement post-stroke," *IEEE Tranctions on Neural System and Rehabilitation Engineering*, vol. 22, no. 4, pp. 886-898, 2014.

[13] B.B. Kang, H. Lee, H. In, U. Jeong, J. Chung, and K.J. Cho, "Development of a polymer-based tendon-driven wearable robotic hand," in *Proceedings of 2016 IEEE International Conference on Robotics and Automation*, Stockholm, Sweden, May 2016, pp. 3750–3755.

[14] D. Popov, I. Gaponov, and J.H. Ryu, "Portable exoskeleton glove with soft structure for hand assistance in activities of daily living," *IEEE/ASME Transactions on Mechatronics*, vol. 22, no. 2, pp. 865–875, 2017.

[15] S. Park, L.Weber, L. Bishop, J. Stein, and M. Ciocarlie, "Design and development of effective transmission mechanisms on a tendon driven hand orthosis for stroke patients," in *Proceedings of 2015 IEEE International Conference on Robotics and Automation*, Brisbane, Australia, May 2018, pp. 2281-2287.

[16] L. Cheng, M. Chen and Z. Li, "Design and control of a wearable hand rehabilitation robot," *IEEE Access*, vol. 6, pp. 74039-74050, 2018.

[17] M. Cempini, M. Cortese, and N. Vitiello, "A powered finger-thumb wearable hand exoskeleton with self-aligning joint axes," *IEEE/ASME Transactions on Mechatronics*, vol. 20, no. 2, pp. 705–716, 2015.

[18] C.J. Nycz, T. Butzer, O. Lambercy, J. Arata, G.S. Fisher, and R. Gassert, "Design and characterization of a lightweight and fully portable remote actuation system for use with a hand exoskeleton," *IEEE Robotics and Automation Letters*, vol. 1, no. 2, pp. 976–983, 2016.

[19] C.L. Jones, F. Wang, R. Morrision, N. Sarkar, and D.G. Kamper, "Design and development of the cable actuated finger exoskeleton for hand rehabilitation following stroke," *IEEE/ASME Transactions on Mechatronics*, vol. 19, no. 1, pp. 131–140, 2014.

[20] P. Agarwal, Y. Yun, J. Fox, K. Madden, and A.D. Deshpande, "Design, control, and testing of a thumb exoskeleton with series elastic actuation," *The International Journal of Robotics Research*, vol. 36, no. 2, pp. 355–375, 2017.

[21] F. Zhang, L. Yang, and Y. Fu, "Design of a novel elastic torque sensor for hand injuries rehabilitation based on bowden cable," *IEEE Transactions on Instrumentation and Measurement*, vol. 68, no. 9, pp. 3184–3192, 2019.

[22] P. Agarwal, J. Fox, Y. Yun, M.K. O'Malley, and A.D. Deshpande, "An index finger exoskeleton with series elastic actuation for rehabilitation: Design, control and performance characterization," *The International Journal of Robotics Research*, vol. 34, no. 14, pp. 1747–1772, 2015.

[23] J. Han, "From PID to active disturbance rejection control," *IEEE Transactions on Industrial Electronics*, vol. 56, no. 3, pp. 900–906, 2009.

[24] Y. Huang and W. Xue, "Active disturbance rejection control: methodology and theoretical analysis," *ISATrans*, vol. 53, no. 4, pp. 963–976, 2014.

[25] Z. Gao, "Scaling and parameterization based controller tuning," in *Proceedings of American Control Conference*, Denver, USA, July 2003, pp. 4989–4996.

[26] H. Li, L. Cheng, W. Li, and W. Xue, "Active disturbance rejection control for a fluid-driven hand rehabiliation device," submitted to *IEEE/ASME Transactions on Mechatronics* for possible publication, 2019.